
**PRODUCTION PROCESSES
AND PROPERTIES OF POWDERS**

Characterization of Ni–Ti Alloy Powders for Use in Additive Manufacturing¹

Gozde S. Altug-Peduk^{a, b, *}, Savas Dilibal^c, Ola Harrysson^a, Sunullah Ozbek^d, and Harvey West^a

^a*Center for Additive Manufacturing and Logistics, Edward P. Fitts Department of Industrial and Systems Engineering,
North Carolina State University, Raleigh, 27607 USA*

^b*Graduate School of Physical Sciences, Istanbul Gedik University, Istanbul, 34876 Turkey*

^c*Engineering Faculty, Department of Mechatronics Engineering, Istanbul Gedik University, Istanbul, 34876 Turkey*

^d*Engineering Faculty, Department of Metallurgical and Materials Engineering, Istanbul Gedik University,
Istanbul, 34876 Turkey*

**e-mail: gsultan.altug@gmail.com*

Received November 3, 2017

Abstract—Additive manufacturing (AM) offers a fully integrated fabrication solution within many engineering applications. Particularly, it provides attractive processing alternatives for nickel-titanium (Ni–Ti) alloys to overcome traditional manufacturing challenges through layer by layer approach. Among powder-based additive manufacturing processes, the laser beam melting (LBM) and the electron beam melting (EBM) are two promising manufacturing methods for Ni–Ti shape memory alloys. In these methods, the physical characteristics of the powder used as raw material in the process have a significant effect on the powder transformation, deposition, and powder-beam interaction. Thus, the final manufactured material properties are highly affected by the properties of the powder particles. In this study, the Ni–Ti powder characteristics are investigated in terms of particle size, density, distribution and chemical properties using EDS, OM, and SEM analyses in order to determine their compatibility in the EBM process. The solidification microstructure, and after built microstructure are also examined for the gas atomized Ni–Ti powders.

Keywords: additive manufacturing, electron beam melting, nickel-titanium alloy, powder characterization

DOI: 10.3103/S106782121804003X

1. INTRODUCTION

Manufacturing technologies are generally classified into three principal categories including subtractive manufacturing technology, formative manufacturing technology, and additive manufacturing technology. While the material is removed by machining processes in order to acquire the desired geometry in subtractive manufacturing technology, the geometry of the part is changed under external forces such as casting, molding, and shaping in formative manufacturing technology. Rather than removing material as in these two methods, the third method involves using additive manufacturing in which the desired geometry of the part is built by adding the material through layer technology [1]. In AM technologies, the material is added layer by layer according to the original computer-aided design (CAD) data in order to produce the actual part. Depending on the applied AM technique, the manufacturing sub-processes, such as preparation of feedstock material, might be different. However, the fabrication basically consists of eight similar stages as

follows; (i) CAD modeling, (ii) STL (Stereolithography) file creation, (iii) file transfer to the AM machine, (iv) machine set up, (v) building, (vi) part removal (vii) post-processing and (viii) application. In this regard, process inputs are described as AM hardware, software, part geometry, scan strategy, build atmosphere and powder quality while process outputs are mechanical and physical properties of the final part as well as geometrical compatibility and elimination of defects [2].

There are different types of AM techniques for layer by layer manufacturing. Among them, the electron beam melting (EBM) utilizes an advanced technology to obtain complex final parts. [1, 3]. The process principle schematically shown in Fig. 1. The electron beam is utilized as the energy source in the process and the entire system and powders are protected from oxidation via vacuum atmosphere. The process starts with preheating the build table. After the preheating stage, actual layer melting process begins with raking of highly spherical metal powders of the 45–100 μm particle fraction onto the build platform [3–5]. After that, the electron beam is accelerated,

¹ The article is published in the original.

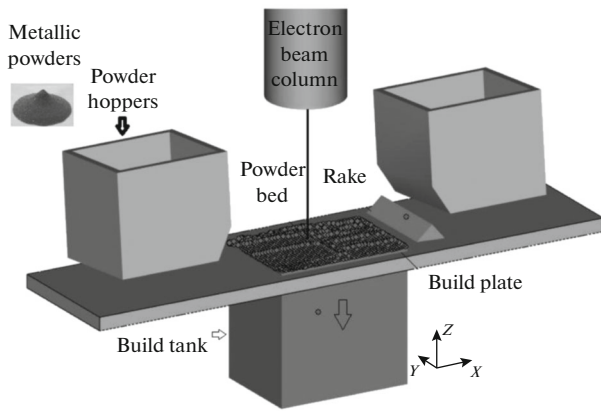


Fig. 1. Schematic illustration of EBM process.

powder particles are melted by the scanning system and following the layer formation, new powder is spread onto the platform to form the second layer at the determined thickness. This cycle repeats as raking, preheating, powder melting and melt post-heating until the desired part is built, according to the CAD design. In the meantime, depending on the process parameters, preheating is carried out by a defocused beam and slightly sintering the powder in order to reduce thermal stresses and obtain smoother melting [6, 7]. Deposition rate of the material is associated with the z -axis layer height or layer thickness. Layer thickness is identified by the powder raking amount. During the 'raking' stage, powder is distributed to the built surface with a metal rake bar. Powder layers should be quite thin in order to obtain bulk structures with complete fusion. Thus during the scanning, the required energy can be easily transferred to the surface by an electron beam to melt the previous layer. Eventually, the value of the layer thickness should be as low as possible in addition to powders with smaller particle size and bimodal size distribution in order to improve the surface quality of the built parts. Therefore, quality of the feedstock powder is seen as one of the most important process inputs which is identified by the powder morphology, size, distribution, flowability, spreadability, composition, and electrical and thermal conductivity [8, 9]. On the other hand, according to the powder atomization methods, powder shapes (irregular, spherical or satellites etc.), size and porosity amount in the built material indicate some variations. Spherical particles and smaller particle sizes improve the flowability and apparent density [10]. Fine and mid fraction powders provide a large surface area which leads to higher energy absorption and higher sintering rate. Among the powder production methods, generally gas or plasma atomization is preferred for EBM, due to the highly spherical shape of the powder, Gaussian type particle size distribution, low oxygen content, good flowability characteristics, high packing density, and powder chemistry [11].

In the gas atomization process, a high-pressure gas is discharged into the chamber in order to disrupt the molten metal stream into fragments and disintegrate into the fine droplets by a further breakup of fragments. The atomization process consists of the three fundamental steps of primary atomization, secondary atomization, and solidification. Regarding the control of particle size and microstructure, the relative velocity between the gas and the liquid metal, melt flow rate, solidification mechanisms and cooling rates are considered as crucial factors. The morphology of gas atomized powder particles tends to be spherical if the spheroidization time of the liquid droplet is shorter than the solidification time (related to the surface tension). Sometimes agglomeration and satellite powders can form owing to the collision in the spray plume between the liquid or semi-liquid droplets and solidified particles. Satellite formation is observed by the circulation of gas within the chamber where the fine particles impact with larger particles [12, 13].

The term shape memory alloys (SMA) refers to a group of intermetallic materials that exhibit reversible shape change upon heating above the austenite final temperature after applying the required thermomechanical treatments [13, 14]. After the discovery of the shape memory and superelastic effects in Ni–Ti alloy, its applications have been expanded in both commercial and industrial fields including biomedical, aerospace, automotive, robotics, mini-actuators, and micro-electromechanical systems [15–19]. Although Ni–Ti SMAs are promising materials, the difficulties on the processing, melting, and machining limit their potential applications [20, 21]. Thus, the production of Ni–Ti alloy with high chemical homogeneity and desired shape-memory properties, especially with complex shapes and geometries is still challenging. Recently, the laser-based additive manufacturing, particularly selective laser melting (SLM), has been utilized in order to produce Ni–Ti shape memory alloys by several researchers [22–24]. Another promising additive manufacturing method is EBM that might offer significantly lower carbon and oxygen concentrations during the processing of Ni–Ti SMAs as well as other microstructural and mechanical advantages. For instance, the penetration depth of an electron beam into the irradiated material is greater than a laser beam due to the available power. The vacuum system in the EBM machines ensures a clean environment and helps to outgas impurities during processing, which is highly important for reactive metals such as Ni and Ti [25]. In the EBM process final part properties are significantly affected by the properties of the powder particles, and machine parameters. Particularly physical and chemical properties of the powder are considered as essential characteristics for material development, and determination of machine parameters. Another advantage of EBM technology are the wide range of materials can be used after sieving in a new process. After building the part, during

Table 1. The results of density and flow rate measurements for the Ni–Ti powder

Apparent density, g/cm ³	Tap density, g/cm ³	Hausner ratio	Flowability index, s/50 g
3.506	4.1485	1.18	20.712

the powder removing step, powders which surrounding the finished part are blasted away in order to recycle into the further processes without causing any material loss [4, 5]. The objective of the present study was to investigate the material characteristics of Ni–Ti alloy powders in order to develop process parameters for their potential application in the EBM based AM technology as well as evaluating powder surface structure for powder recyclability.

2. MATERIALS AND METHODS

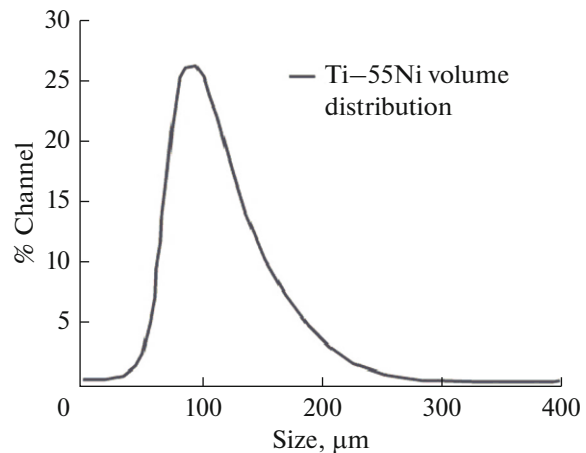
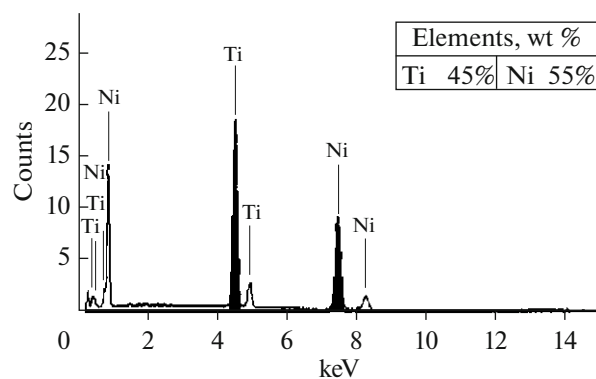
The gas atomized, pre-alloyed Ti–55 wt % Ni powder which was provided by the ATI Company (USA) in the range of –100/+325 mesh (44–149 μm) particle size was used for the characterization of Ni–Ti powders. In the first stage, the tap density, apparent density, and flow rate values were determined. Tap density and apparent density measurements were performed at 22.8°C in accordance with the ASTM B527-14 and ASTM B703-10 standards, respectively [26, 27]. The tap density measurements have been performed with 100 ml of powder subjected to 3000 taps. And then, the flow rate was performed with a Hall flowmeter funnel using the static flow method in accordance with ASTM B213 standard [28]. In the second stage, the particle size distribution was defined with a laser diffraction analysis technique using a Microtrac S3500 particle size analyzer. This analysis was carried out in Triton-X surfactant and the results were evaluated based on volume distribution with mass median diameter D50 value which is defined as the powder size that corresponds to the 50% cumulative frequency. The morphological features of the powder were analyzed using Hirox KH7700 digital optical microscope and Jeol 6010LA scanning electron microscope. Additionally, the relationship between particle microstructures and physical properties was analyzed. Some of the powders were hot mounted in phenolic resin, ground, polished, and etched with Kroll's reagent (2% HF, 5% HNO₃, 93% distilled water) for the cross section examinations.

3. EXPERIMENTAL RESULTS

The experimental results of powder density, flow rate, particle size distribution and microstructural characterization of powders were elaborated in this section. In terms of powder density and flowability, the powder was observed to have good flowability characteristics as shown in Table 1. The Hausner ratio was determined to be within the acceptable range for the AM process. The ratio of the tap density to the

apparent density (Hausner ratio) indicates the powder flowability characteristic. This ratio is expected to be less than 1.25 for metallic powders for appropriate flowability and packing density properties for metallic powders. The obtained median size distribution of gas atomized Ni–Ti powders was 92.48 μm as shown in Fig. 2.

The EDS analysis was applied for the Ni–Ti powder, and revealed that it was pre-alloyed with 45 Ti to 55 Ni elemental weight ratio as shown in Fig. 3. Considering the Ni–Ti phase diagram, the obtained Ti–55 wt % Ni composition corresponds to equal atomic percentage for Ni and Ti elements. The morphological examinations in OM image observed that the mid fraction and fine powder particles are of spherical shape in low magnification as shown in Fig. 4a. In addition, the SEM image showed that most of the par-

**Fig. 2.** Particle size volume distribution of Ni–Ti powders.**Fig. 3.** EDS analysis result of Ni–Ti powders.

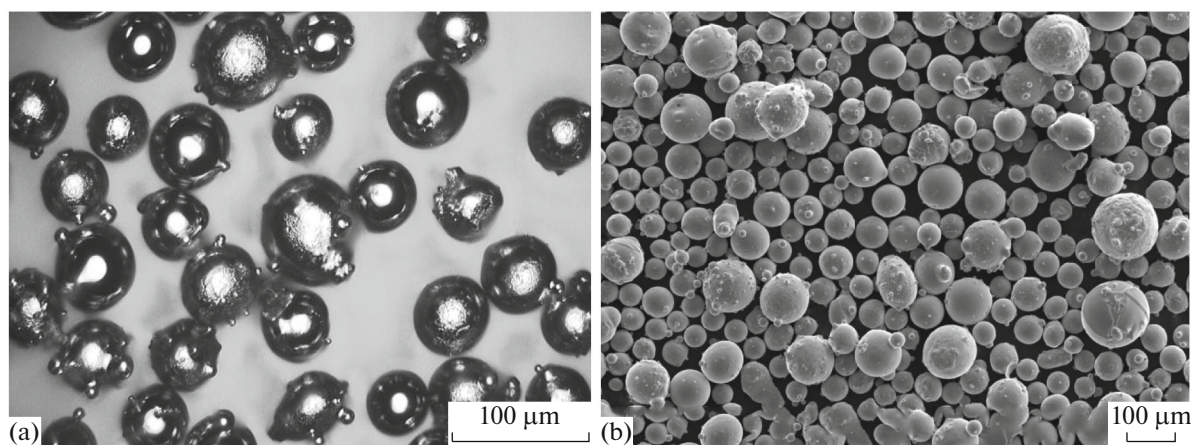


Fig. 4. Low magnification: (a) OM image, (b) SEM image of Ni–Ti powders.

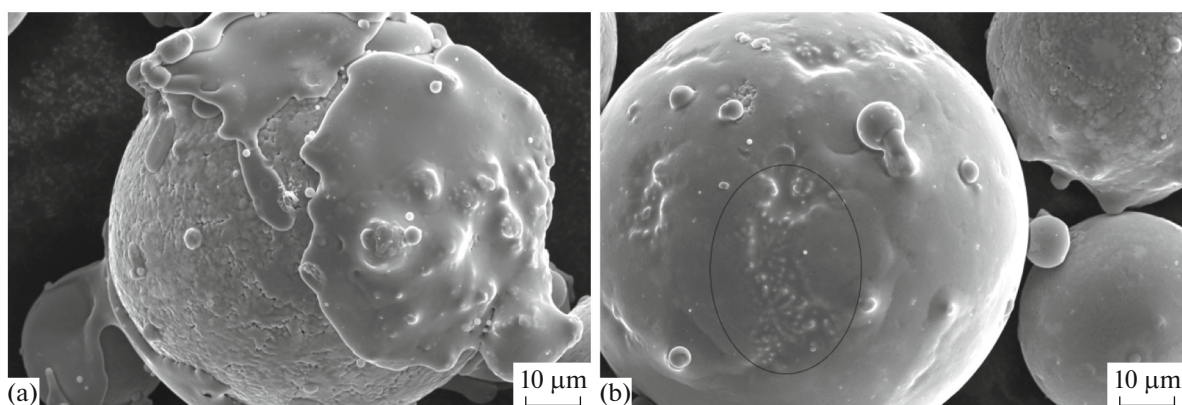


Fig. 5. Higher magnification SEM image of Ni–Ti powders (a) Splat cap formation on the both large and attached satellite particle, (b) the dendritic fragments in the selected area.

ticles contain smaller attached ‘satellite’ particles on their surfaces as seen in Fig. 4b. The particle size volume distribution result plotted in Fig. 2 was shown that the particles were within the desired range.

As a result of the detailed microstructural examinations using SEM in higher magnifications, dendritic fragments were found on a smooth powder surface as revealed in the circle in addition to the evidence of satellite formation and the polycrystalline structure as shown in Fig. 5b. A cross-sectional investigation was applied to some of the samples to identify the nucleation and solidification behaviors. In the case of a small liquid droplet colliding with a large cold particle, partial covering of splatted material (splat cap) is revealed on the larger particle as clearly seen in Fig. 5a.

In our study, the presence of dendritic structures was determined as the dominant morphology in the cross-sectional microstructures from the etched powder surfaces. Additionally, some of the powders particularly with splat cap and $<10\ \mu\text{m}$ attached particles on their surfaces, illustrated partially cellular structure

formation as seen in Fig. 6a. The higher magnification image of a spherical powder was examined in Fig. 6b. The SEM micrographs of etched Ni–Ti powders results were indicated that the growth of grains originated from nucleation sites on the melt droplet surface. Since satellite particles had already been solidified before the collision, finer microstructures were observed on the interface and inner side of the particle. In some regions, dendritic fragments were found as divided and distributed in the matrix.

For this specific NiTi powder, optimized processing parameters are not available from the machine manufacturer (Arcam). In the light of the powder characteristics, EBM process parameters (layer thickness, scanning speed, beam current, energy density) were developed and optimized for Ti55Ni alloy. EBM process begins with raking powder and repeated as raking, preheating, powder melting and post-heating throughout the build for each layer. Layer thickness is identified by the powder raking amount. During the ‘raking’ stage, the powder is distributed to the built surface with a metal rake bar. In this study $50\ \mu\text{m}$ layer

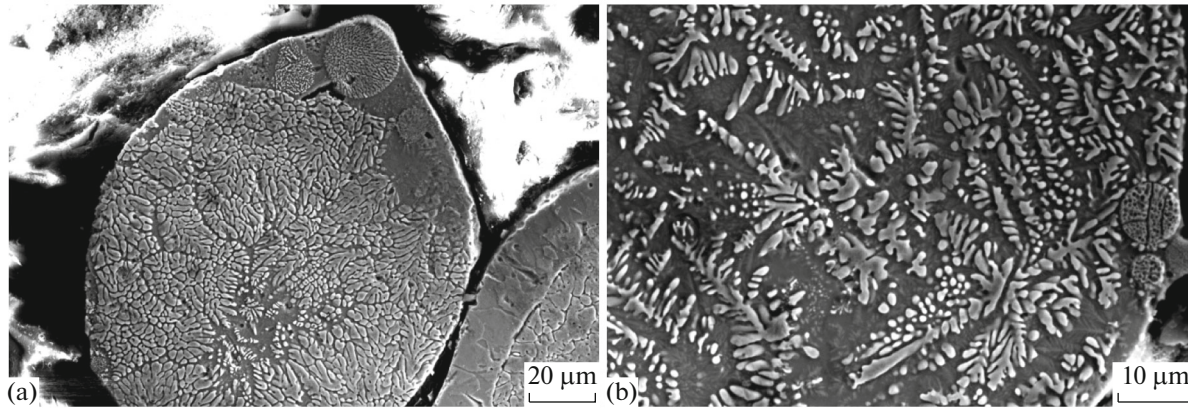


Fig. 6. Cross-sectional SEM micrographs of etched Ni–Ti powders; (a) the microstructure, (b) dendritic solidification direction in the spherical powder.

thickness were selected. In the preheating stage soft sintering, and then smoother melting were obtained on the whole powder area. After the 6 h building process in Arcam Q10Plus machine, the microstructure of slightly sintered, and unmelted NiTi powders were examined (Fig. 7).

4. DISCUSSION

Powder morphology, internal friction, and powder size distribution are the main effective factors on the apparent density and flow rate properties. Highly spherical particles with low interparticle friction are preferred in order to achieve desired flowability and layer deposition characteristics for additive manufacturing. The contact surface between the coarse particles is relatively lower than the fine particles which generate less inter-particle friction. Thus, apparent density reduces with increasing particle size in contrast to flow rate which is restricted with the increasing friction between the particles. The flow of particles is inherently carried out by forces between the particles. Yablokova and coworkers [29] examined the flowability characteristics of Ni–Ti powders. Similar to the current work, they observed that Ni–Ti powders with the 45–100 μm particle fraction as well as spherical morphologies showed high flowability. In EBM process, the particle size affects the layer thickness values. Additionally, the maximum particle size causes the formation of rough surfaces on the part. In order to enhance powder bed density as well as flowability, narrow particle size distributions by a majority of spherical particles are demanded.

The gas atomization process was made using high cooling rates because of the initial high relative velocity of the droplets and the fast moving cold gas stream. We note that the particle size and cooling rates dictate the obtained form of the microstructures, such as amorphous, supersaturated or well-developed forms. Similar results were observed in a recent study of Zong

et al. [30]. They observed a fine dendrite structure with gas atomization powders due to the high cooling rates. The effect of atomization on solidification was also investigated by Behulova et al. [31]. A mixture of dendritic and grain refined morphology was detected in their study.

In the SEM results, it was detected that some of the powders illustrated partially cellular structure formation. This might be due to the solidification under-cooling and much faster heat extraction from the interface of the bigger droplet through the already solidified cooler satellite particle [32].

To investigate the microstructure of the recycled powders, the high resolution SEM micrograph results were examined during the experimental analysis. We note that the recycled powder can be reused after a sieving process which eliminates the deformed spherical powders. After the sieving process, the remaining powders can be blended with a small amount of gas atomized powder with lower oxygen content. After

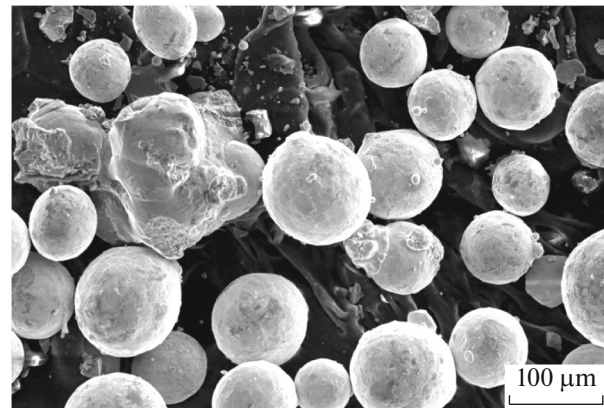


Fig. 7. Microstructure of powders after EBM building process.

finishing these procedures, they can be used in a new EBM building process.

5. CONCLUSIONS

In this study, the main NiTi powder requirements for the EBM based additive manufacturing were investigated in terms of particle size, density, size distribution and chemical properties. For this purpose, OM, SEM and EDS analyses were conducted systematically after powder flowability and particle size distribution analysis. Spherical powder structures with homogenous particle size distribution have been observed in the microscopic examination. A high packing density has been obtained from the gas atomization process. Additionally, detailed microstructure analysis revealed that the dendritic solidification fragment was distributed in the matrix. Furthermore, a homogenous slightly sintered microstructure has been obtained after 6 h building process in EBM machine. Although surface deformation was occurred on the some of the powders due to the blasting of the powder through EBM building process, this study observed that after the elimination of the agglomerated powders, NiTi powders satisfy the appropriate conditions for reusing in the EBM process. Geometrical conformity of the manufactured part is directly related to layer thickness. Selected powder layer thickness value, provided a tighter bonding in between the powders. Thus during the scanning, the required energy can easily be transferred to the surface by an electron beam to melt the layers. Therefore, it is concluded that in order to improve the surface quality of the EBM NiTi built parts, layer thickness values should be as low as possible in addition to powders with smaller particle size and Gaussian distribution. The thermomechanical characteristics of the EBM processed Ni–Ti SMA will be investigated in the future study.

ACKNOWLEDGMENTS

The work described in this paper has been supported by the Center of Additive Manufacturing and Logistics, North Carolina State University, Raleigh, NC, USA. The authors are greatly thankful to ATI Specialty Materials for providing the materials used in this study.

REFERENCES

- Gebhardt, A., and Butter, J.S., *3D Printing for Prototyping and Manufacturing*, Hanser, 2016.
- Sames, W.J., List, F.A., Pannala, S., Dehoff, R.R., and Babu, S.S., The metallurgy and processing science of metal additive manufacturing, *Int. Mater. Rev.*, 2016. doi 10.1080/09506608.2015.1116649
- Karlsson, J., Optimization of Electron Beam Melting for Production of Small Components in Biocompatible Titanium Grade, *Ph.D. Thesis*, Uppsala Univ., 2015.
- Cansizoglu, O., Mesh Structures with Tailored Properties and Applications in Hip Stems, *Ph.D. Thesis*, North Carolina State Univ., 2008.
- Horn, T.J., and Harrysson, O.L.A., Overview of current additive manufacturing technologies and selected applications, *Sci. Prog.*, 2012, vol. 95, no. 3, pp. 255–282.
- Cormier, D., Harrysson, O.L.A., and West, H., Characterization of H13 steel produced via electron beam melting, *Rapid Prototyp. J.*, 2004, vol.10, no. 1, pp. 35–41.
- Cheng, X.Y., Li, S.J., Murr, L.E., Zhang, Z.B., Hao, Y.L., Yang, R., Medina F., and Wicker, R.B., Compression deformation behavior of Ti–6Al–4V alloy with cellular structures fabricated by electron beam melting, *J. Mech. Behav. Biomed. Mater.*, 2012, vol. 16, pp. 153–162.
- Sutton, A.T., Kriewall, C.S., Leu, C.M., and Newkirk, J.W., Powders for additive manufacturing processes: characterization techniques and effects on part properties, in *Solid Freeform Fabrication 2016: Proc. 26th Ann. Int. Solid Freeform Fabrication Symp.—An Additive Manuf. Conf.*, Texas: AT&T Conf. Center, 2016, pp. 1004–1030.
- Slotwinski, J.A., Garboczi, E.J., Stutzman, P.E., Ferraris, C.F., Watson, S.S., and Peltz M.A., Characterization of metal powders used for additive manufacturing, *J. Res. Nat. Inst. Stand. Technol.*, 2014, vol. 119, pp. 460–493.
- Elahinia, M.H., Moghaddam, N.S., Andani, M.T., Amerinatanzi, A., Bimber, B.A., and Hamilton, R.F., Fabrication of NiTi through additive manufacturing: A review, *Prog. Mater. Sci.*, 2016, vol. 83, pp. 630–663.
- Robertson, I.M. and Schaffer, G.B., Some effects of the particle size on the sintering of titanium and a master sintering curve model, *Metall. Mater. Trans.*, 2009, vol. 40A, no. 8, pp. 1968–1979.
- Wong, K.V., and Hernandez, A., A review of additive manufacturing, *ISRN Mech. Eng.*, 2012. doi 10.5402/2012/208760
- Dilibal, S., Investigation of nucleation and growth of detwinning mechanism in martensitic single crystal NiTi using digital image correlation, *Metallography, Microstr., Anal.*, 2013, vol. 2, no. 4, pp. 242–248.
- Elahinia, M., Hashemi, M., Tabesh, M., and Bhaduri, S.B., Manufacturing and processing of NiTi implants: A review, *Prog. Mater. Sci.*, 2012, vol. 57, pp. 911–946.
- Kauffman, G.B., The story of nitinol: the serendipitous discovery of the memory metal and its applications, *The Chem. Educ.*, 1996, vol. 2, no. 2, pp. 3–21.
- Mohd Jani, J., Leary, M., Subic, A., and Gibson, M.A., A review of shape memory alloy research, applications and opportunities, *Mater. Des.*, 2014, vol. 56, pp. 1078–1113.
- Engeberg, E.D., Dilibal, S., Vatani, M., Choi, J.W., and Lavery, J., Anthropomorphic finger antagonistically actuated by SMA plates, *Bioinspir. & Biomimet.*, 2015, vol. 10, 056002.
- Moghaddam, N. S., *Toward Patient Specific Long Lasting Metallic Implants for Mandibular Segmental Defects*, Master Thesis, Toledo (OH): Univ. of Toledo, 2015.

19. Haberland, C., Elahinia, M., Walker, J., Meier, H., and Frenzel, J., On the development of high quality NiTi shape memory and pseudoelastic parts by additive manufacturing, *Smart Mater. Struct.*, 2014, vol. 23, p. 104002.
20. Guo, Y., Klink, A., Fu, C., and Snyder, J., Machinability and surface integrity of Nitinol shape memory alloy, *CIRP Ann.—Manuf. Technol.*, 2013, vol. 62, no. 1, pp. 83–86.
21. Moghaddam, N.S., Skoracki, R., Miller, M., Elahinia, M., and Dean, D., Three dimensional printing of stiffness-tuned, nitinol skeletal fixation hardware with an example of mandibular segmental defect repair, *Proc. CIRP*, 2016, vol. 49, pp. 45–50.
22. Walker, J.M., Additive Manufacturing Towards the Realization of Porous and Stiffness-Tailored NiTi Implants, *Ph.D. Thesis*, Toledo (OH): Univ. of Toledo, 2014.
23. Halani, P.R., Kaya, I., Yung, C., Shin, Y.C., and Karaca, H.E., Phase transformation characteristics and mechanical characterization of nitinol synthesized by laser direct deposition, *Mater. Sci. Eng. A*, 2013, vol. 559, pp. 836–843.
24. Meier, H., Haberland, C., and Frenzel, J., *Structural and Functional Properties of NiTi Shape Memory Alloys Produced by Selective Laser Melting, Innovative Developments in Design and Manufacturing: Advanced Research in Virtual and Rapid Prototyping*, London: CRC, 2011.
25. Murr, L.E., Metallurgy of additive manufacturing: Examples from electron beam melting, *Add. Manuf.*, 2015, vol. 5, pp. 40–53.
26. *ASTM Standard, ASTM B527–15, Standard Test Method for Tap Density of Metal Powders and Compounds*, West Conshohocken (PA): ASTM Int., 2014.
27. *ASTM Standard, ASTM B703–10, Standard Test Method for Apparent Density of Metal Powders and Related Compounds Using the Arnold Meter*, West Conshohocken (PA): ASTM Int., 2010.
28. *ASTM Standard, ASTM B213–13, Standard Test Methods for Flow Rate of Metal Powders Using the Hall Flowmeter Funnel*, West Conshohocken (PA): ASTM Int., 2013.
29. Yablokova, G., Speirs, M., Van Humbeeck, J., Kruth, J.P., Schrooten, J., Cloots, R., Boschini, F., Lumay, G., and Luyten, J., Rheological behavior of β -Ti and NiTi powders produced by atomization for SLM production of open porous orthopedic implants, *Powder Technol.*, 2015, vol. 283, pp. 199–209.
30. Zhong, C., Chen, J., Linnenbrink, S., Gasser, A., Sui, S., and Poprawe, R., A comparative study of Inconel 718 formed by high deposition rate laser metal deposition with GA powder and PREP powder, *Mater. Des.*, 2016, vol. 107, pp. 386–392.
31. Behulova, M., Moravcik, R., Kusy, M., Caplovic, L., Grgac, P., and Stancek, L., Influence of atomization on solidification microstructures in the rapidly solidified powder of the Cr–Mo–V tool steel, *Mater. Sci. Eng. A*, 2001, vol. 304, pp. 540–543.
32. Hong, S.J., Etching effect on microstructural behavior of gas atomized Al-20 mass%Si alloy powder, *Mater. Trans.*, 2010, no. 5, pp. 1055–1058.